Enzymatic Biodegradability of Pristine and Functionalized Transition Metal Dichalcogenide MoS_2 Nanosheets

*Rajendra Kurapati, Laura Muzi, Aritz Perez Ruiz de Garibay, Julie Russier, Damien Voiry, Isabella A. Vacchi, Manish Chhowalla, and Alberto Bianco**

2D transition metal dichalcogenide MoS_2 nanosheets are increasingly attracting interests due to their promising applications in materials science and biomedicine. However, their biocompatibility and their biodegradability have not been thoroughly studied yet. Here, the biodegradability of exfoliated pristine and covalently functionalized MoS_2 (*f*-MoS_2) is investigated. First, biodegradability of these nanomaterials is evaluated using plant horseradish peroxidase and human myeloperoxidase. The results reveal that the enzymatic degradability rate of MoS_2 and *f*-MoS_2 is slower than in the case of the simple treatment with H_2O_2 alone. In parallel, high biocompatibility of both pristine and *f*-MoS_2 nanosheets is found up to 100 µg mL^{-1} in both cell lines (HeLa and Raw264.7) and primary immune cells. In addition, no immune cell activation and minimal pro-inflammatory cytokine release are observed in RAW264.7 and human monocyte-derived macrophages, suggesting a negligible cellular impact of such materials. Furthermore, the effects of degraded MoS_2 and partially degraded *f*-MoS_2 products on cell viability and activation are studied in cancer and immune cells. A certain cytotoxicity is measured at the highest concentrations. Finally, to prove that the cellular impact is due to cell uptake, the internalization of both pristine and functionalized MoS_2 in cancer and primary immune cells is assessed.

1. Introduction

2D transition metal dichalcogenides (TMDCs) like MoS_2 are the second most studied layered materials after graphene.[1] TMDCs have unique physicochemical properties, thus attracting enormous interest for the next generation of electronic and optoelectronic devices, for catalysis, for sensing, for energy storage, etc.[1,2] Related to these applications, there is a serious concern about the stability or degradability of TMDCs in air and aqueous media. Indeed, the stability of such nanomaterials can influence their behavior in the different types of envisaged uses.[3–5] MoS_2 is considered relatively chemically inert in ambient conditions. However, its chemical stability, optical and electrical properties are dependent on its crystalline phase. The most common crystalline phase of MoS_2 is the trigonal prismatic (2H phase). In this phase, MoS_2 acts as semiconductor, while in the orthogonal phase (1T phase) MoS_2 acts as metal.[6] MoS_2 in 1T phase is more reactive than in 2H phase, the latter being inert toward most of the chemicals. Indeed, the difference in their electronic states dictates the chemical reactivity of these two crystalline forms of MoS_2. Although metastable, it has been shown that 1T phase of MoS_2 can be stabilized by insertion of Li^+ ions into its crystal lattice, and recently covalent functionalization resulted also effective in stabilizing this phase.[7] Earlier, Voiry et al. reported a simple and efficient route for covalent functionalization of MoS_2 sheets facilitated by electron transfer between electron-rich metallic 1T phase and organohalides leading to semiconducting MoS_2.[7] Covalent functionalization of MoS_2 sheets was also achieved by exploiting the reactivity of surface and edge defects.[8] The defects on the lattice of MoS_2 were modified, for example, by functionalization with thiols leading to MoS_2 sheets with tuned electronic properties.[8] Alternatively, electron transfer characteristics of MoS_2 can be altered by complexation between MoS_2 layers and optoelectronically active molecules like phthalocyanines.[9]

Besides the development for electronics, optoelectronics, and catalytic applications, to mention few of them, biomedical applications of exfoliated TMDCs are increasingly attracting the attention as promising alternatives to graphene. This is mainly due to their high biocompatibility compared to other nanomaterials and strong contrast properties because of the presence of heavy elements like Mo, W, Bi, etc.[3] In this context, TMDCs showed high potential in drug delivery, cancer theranostics, antimicrobials, bioimaging, and biosensing.[3,10–12] Near-infrared light-mediated multimodal cancer theranostics based on TMDCs seems to be more promising for biomedicine due to higher photothermal conversion ability as well as stronger contrasting nature over carbon nanomaterials.[3] However, a limited number of data on toxicity are available, while

Dr. R. Kurapati, Dr. L. Muzi, Dr. A. P. R. de Garibay, Dr. J. Russier, I. A. Vacchi, Dr. A. Bianco
University of Strasbourg, CNRS
Immunopathology and Therapeutic Chemistry, UPR 3572
67000 Strasbourg, France
E-mail: a.bianco@ibmc-cnrs.unistra.fr
Dr. D. Voiry,[+] Prof. M. Chhowalla
Materials Science and Engineering
Rutgers – The State University of New Jersey
607 Taylor Road, Piscataway, NJ 08854, USA

[+]Present address: IEM (Institut Européen des Membranes), UMR 5635, Université de Montpellier, CNRS, ENSCM, F-34095 Montpellier, France

DOI: 10.1002/adfm.201605176

the enzymatic degradability of TMDCs has not been studied yet.[13,14] A few studies showed that MoS_2 displays better biocompatibility than graphene or graphene oxide, but this needs to be confirmed by further works.[15–17] A recent study demonstrated that the cytotoxicity of MoS_2 depends on its aggregation state and the extent of exfoliation.[13] Highly dispersed MoS_2 sheets were not cytotoxic compared to aggregated sheets, while highly exfoliated sheets induced higher cell mortality compared to moderately exfoliated sheets.[13] From a clinical point of view, any nanomaterials, either as vehicle to carry therapeutic molecules or as implanted material in regenerative medicine, should be excreted from the body or biodegraded.[18]

It is known that MoS_2 can be decomposed in the presence of H_2O_2.[19] Since, hydrogen peroxide is a ubiquitous molecule, we thought that it could be interesting to evaluate the decomposition or degradation of MoS_2 sheets at physiological concentrations of H_2O_2. On the other hand, an increased secretion of reactive oxygen species (ROS) including superoxide ($O_2^{\bullet-}$), hydroxy radicals ($HO^{\bullet}$), and hydrogen peroxide occurs in cancer tissues or in inflammatory conditions.[20–22] High amounts of ROS are caused by oncogene stimulation, malfunction of mitochondria, and chronic inflammation.[22] ROS affect the proteins which control the redox balance, leading to high production of H_2O_2.[20,22] The concentration of ROS in tumor cells is ≈100 times more than in normal cells.[23] Since $50–100 \times 10^{-6}$ M of H_2O_2 concentration are more biologically relevant concentration, H_2O_2-responsive anticancer drug delivery systems have been recently designed.[24–26] In this context, we considered important to study the stability of MoS_2 sheets under similar oxidative conditions to reveal their potential as biodegradable nanocarriers for drug delivery applications.

Having in mind the possibility to extend the use of TMDC materials in biomedicine, we have thus decided to investigate the biocompatibility and biodegradability of MoS_2. For this purpose, we have selected two types of highly water dispersible MoS_2 samples, namely, metastable pristine MoS_2 and covalently functionalized and highly stable *f*-MoS_2, respectively.[7] We started to evaluate the biodegradation of MoS_2 materials by model peroxidase enzyme horseradish peroxidase (HRP), human myeloperoxidase (MPO), and by hydrogen peroxide alone. We then studied the cytotoxicity of these materials using two different cell lines and primary immune cells (hMDMs, human monocyte-derived macrophages). We used HeLa cells as both epithelial and cancer cell model and RAW 264.7 macrophages as immune and phagocytic model. hMDMs were obtained from peripheral blood mononuclear cells (PBMC) from healthy donors and used to address the overall effect of MoS_2 and *f*-MoS_2 toward primary immune cells. We carried out cell viability and pro-inflammatory activation tests to measure key cytotoxicity parameters. Then, we studied the cytotoxicity of byproducts obtained during the process of biodegradation of MoS_2 and *f*-MoS_2 using hydrogen peroxide. Finally, we analyzed the uptake of these two materials in cultured cells, and characterized the membrane interaction and the intracellular presence of pristine and *f*-MoS_2 using transmission electron microscopy (TEM). Overall, this report provides a full comprehensive study on cytotoxicity, biodegradability, and impact of degradation byproducts of pristine and functionalized MoS_2.

2. Results and Discussion

Biodegradation of carbon-based materials was demonstrated by treating them with different types of peroxidases and oxidative enzymes in the presence of low concentration of hydrogen peroxide.[27–32] More recently, we have shown that even 2D materials like hexagonal boron nitride (hBN) nanosheets undergo enzymatic degradation.[33] Unlike graphene and hBN, layered MoS_2 is an unstable material in ambient conditions (room temperature and atmospheric pressure). In fact, it has been shown that MoS_2 is subjected to environmental degradation over a period of several months.[4] The slow oxidation of MoS_2 sheets was observed in the presence of moisture and oxygen.[4] In this direction, we believe that it is very important to study the biodegradability of such sensitive MoS_2 sheets under physiological conditions using different peroxidases and biological concentrations of H_2O_2 to assess possible issues related to biopersistence of this type of 2D materials. Thus, we investigate the capacity of different oxidative enzymes to degrade pristine MoS_2 and MoS_2 covalently functionalized with acetamide groups. Pristine MoS_2 nanosheets and acetamide *f*-MoS_2 (Figure S1A,B, Supporting Information) were synthesized and characterized according to our previous work.[7] Pristine MoS_2 sheets containing a large fraction of electron-rich 1T phase crystals were synthesized by chemical exfoliation and the covalent functionalization of MoS_2 was subsequently obtained by treating MoS_2 with 2-iodoacetamide (see the Supporting Information for details about the synthesis and characterization of MoS_2 and *f*-MoS_2 nanosheets, Figure S1C–H, Supporting Information).[7] The functional groups were covalently bound to S atoms [via S—C bond formation, confirmed by X-ray photoelectron spectroscopy (XPS) analyses, Figure S1] transforming the metallic phase of MoS_2 sheets into semiconducting state.[7] Pristine and *f*-MoS_2 were characterized by additional techniques including scanning transmission electron microscopy (STEM), TEM, and Raman (Figures S1 and S2, Supporting Information). Both types of MoS_2 possess excellent colloidal stability in water, as supported by the values of their zeta potentials, corresponding to −47 mV for MoS_2 and −43.6 mV for *f*-MoS_2 at pH 7, respectively. Following the synthesis and characterization, we treated these nanomaterials with horseradish peroxidase, myeloperoxidase, or with only biological concentrations of hydrogen peroxide.

2.1. Degradation by HRP

To assess the oxidative effect of peroxidases, pristine and *f*-MoS_2 at 100 μg mL^{-1} were first incubated with HRP in phosphate buffer saline (PBS). H_2O_2 was added (to the final concentration of 40×10^{-6} M) to both suspensions once per day up to 30 d. The dilution of the samples into PBS initially transformed the stable colloidal water suspensions into blackish aggregated suspensions (Figure S3A,E, Supporting Information). After 20 d these suspensions turned into pale brownish in the case of pristine MoS_2 (Figure S3C, Supporting Information), while it remained still blackish for *f*-MoS_2 (Figure S3G, Supporting Information). Surprisingly, the color of both MoS_2 and *f*-MoS_2 control samples treated only with H_2O_2, became nearly translucent after 20 d (Figure S3D,H, Supporting Information). We

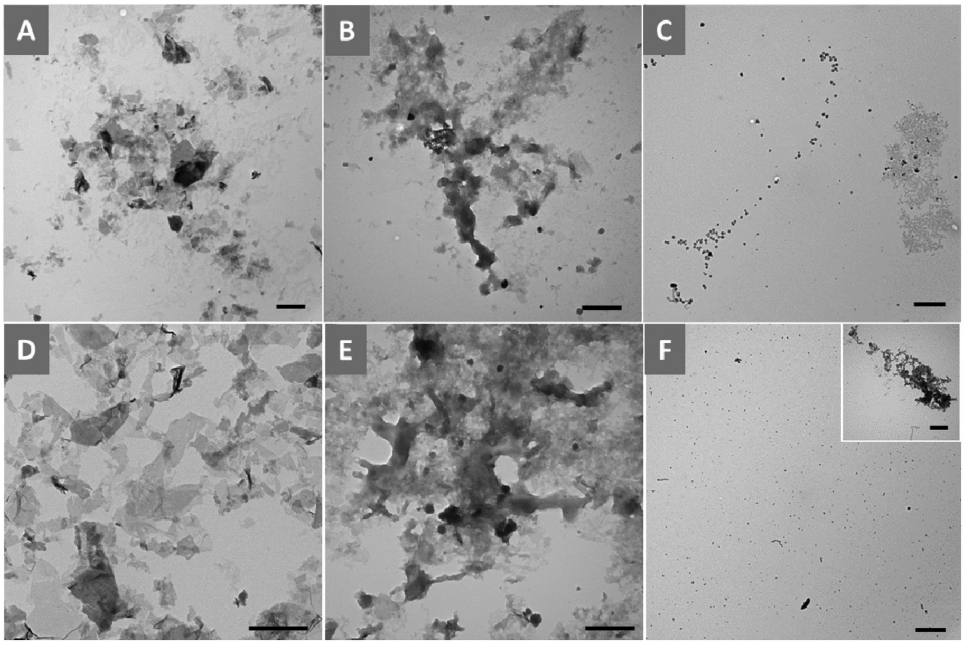

Figure 1. TEM images. A) MoS_2 sheets dispersed in water; B) 20 d treated MoS_2 sheets with HRP+H_2O_2; C) 20 d treated MoS_2 sheets only by addition of H_2O_2; D) *f*-MoS_2 sheets dispersed in water; E) 20 d treated *f*-MoS_2 sheets with HRP+H_2O_2; and F) 20 d treated *f*-MoS_2 sheets only by addition of H_2O_2. Inset in (F) shows partially degraded nanosheets. Scale bars represent 500 nm in all images.

decided then to employ TEM to get more insights about the degradation process. As shown in **Figure 1**B,E, both MoS_2 and *f*-MoS_2 sheets were only partially degraded after 20 d treatment in comparison to the starting materials (Figure 1A,D). The control samples treated only with H_2O_2 were instead almost completely degraded in the same period leading to the formation of spherical nanoparticles with size varied from ≈20 to 50 nm (Figure 1C,F). However, in the case of *f*-MoS_2 we could still observe the presence of some partially degraded nanosheets (Figure 1F, inset). Overall, the treatment with HRP/H_2O_2 revealed that the degradation of both MoS_2 nanosheets is completely different from carbon nanomaterials, where nearly full degradation (transparent solutions) was observed using HRP.[29,34,35] Interestingly, the treatment with H_2O_2 resulted in the complete decomposition of MoS_2 or *f*-MoS_2 nanosheets into nanoparticles, opposite to the results with carbon nanomaterials, where H_2O_2 did not affect their morphology.[28,30,34] In addition, we observed that functionalized MoS_2 was degraded more slowly than pristine material, likely due to the stabilization of the latter by covalent functionalization.[7]

2.2. Degradation by Human MPO

In the next step, both MoS_2 and *f*-MoS_2 samples at 100 µg mL^{-1} were treated with human MPO, an enzyme overexpressed in activated immune cells (e.g., neutrophils), in the presence of NaCl and H_2O_2. In this case, H_2O_2 was added to a final concentration of 200×10^{-6} M every hour up to 24 h. The color of pristine MoS_2 suspension changed to nearly translucent after treating with the enzyme for 24 h (Figure S4, Supporting Information, left vials). However, the decomposition of MoS_2 occurred already after 15 h treatment with only H_2O_2. *f*-MoS_2 suspension also changed to nearly clear solution after treatment with MPO/H_2O_2/NaCl for 24 h (Figure S4, Supporting Information, right vials). Again a quick decomposition of *f*-MoS_2 leading to an almost clear solution occurred by treating with only H_2O_2 after 15 h. TEM analyses were performed to obtain more details about the morphology of MoS_2 and *f*-MoS_2 remaining materials after the treatment with MPO. Pristine MoS_2 sheets were completely decomposed into tiny fragments after 24 h (**Figure 2**B). In addition, the layered-like morphology of MoS_2 was entirely lost after treating with only H_2O_2 for 15 h (Figure 2C). Similarly, most of the *f*-MoS_2 sheets were also broken down into small fragments and partially degraded sheets (Figure 2E) after treatment with the enzyme. Instead, mostly nanoparticles were formed from the treatment with H_2O_2 for 20 h (Figure 2F). Overall, TEM results revealed that the degradation of both MoS_2 samples was slowed down in the case of MPO/NaCl/H_2O_2 compared to the treatment with H_2O_2 alone. This is in agreement with the results obtained with HRP. In addition, covalently functionalized nanosheets displayed a higher stability compared to pristine MoS_2 sheets in both enzymatic process using HRP and MPO, respectively (Figures 1 and 2).

2.3. Degradation by Hydrogen Peroxide

After proving a direct impact of hydrogen peroxide on the degradation process of MoS_2 and *f*-MoS_2 (Figures 1 and 2), we have decided to investigate the stability of both materials in the presence of various concentrations of H_2O_2. Earlier studies revealed that MoS_2 is very sensitive to H_2O_2. Thus, we treated MoS_2 and *f*-MoS_2 sheets with H_2O_2 (added only once at day 0 and incubated for 30 d at 37 °C, see the Supporting

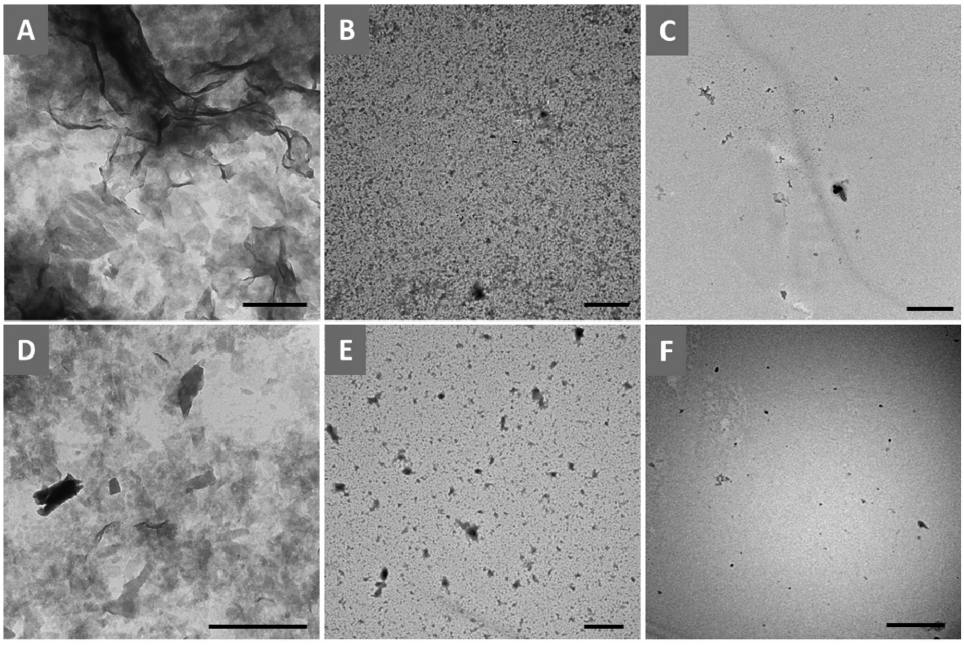

Figure 2. TEM images. A) MoS_2 sheets dispersed in PBS after 24 h; B) 24 h treated MoS_2 sheets with MPO/NaCl/H_2O_2; C) 15 h treated MoS_2 sheets by addition of only H_2O_2; D) *f*-MoS_2 sheets dispersed in PBS after 24 h; E) 24 h treated *f*-MoS_2 sheets with MPO/NaCl/H_2O_2; and F) 20 h treated *f*-MoS_2 sheets by addition of only H_2O_2. Scale bars represent 500 nm in all images.

Information for details) varying the concentration from 10×10^{-6} to 2×10^{-3} M. This range of concentrations corresponds to that found in normal or physiological altered cells and tissues. Indeed, metabolic activity of cancer cells and activated immune cells produce high amounts of ROS, especially H_2O_2.[24,26,36] Our results revealed a concentration- and time-dependent decomposition of pristine MoS_2 (Figure S5, Supporting Information), since the black color of MoS_2 suspensions gradually disappeared by increasing the concentration of H_2O_2 as well as the incubation time. As displayed in Figure S5 (Supporting Information), MoS_2 suspension almost turned into colorless by 14 d treatment even with low concentration of H_2O_2 (10×10^{-6} M). Surprisingly, MoS_2 sheets also slowly decomposed in PBS. In line with this finding, very recently a study has revealed that MoS_2 materials are unstable and undergoes oxidative dissolutions in simply air-saturated solutions.[37,38] On the other hand, *f*-MoS_2 showed greater stability in H_2O_2 compared to the pristine MoS_2 (Figure S6, Supporting Information). Also in this case there was a concentration- and time-dependent decomposition. However, this was much slower compared to pristine MoS_2. Even after 30 d, *f*-MoS_2 suspension did not change completely the color. In addition, the stability of *f*-MoS_2 in PBS was much higher. As most of the metastatic cancer cells contain H_2O_2 at concentrations between 50 and 100×10^{-6} M,[24,26] we decided to analyze both pristine and functionalized MoS_2 samples at 50×10^{-6} M of H_2O_2 of up to 30 d (Figure S7, Supporting Information). TEM analyses indicated that pristine MoS_2 sheets decomposed nearly completely by 14 d incubation (**Figure 3**A,B), where nanoparticles were mostly observed (Figure 3B) along with some partially degraded sheets (Figure 3A). In contrast, *f*-MoS_2 sheets were degraded only partially even after 30 d in contrast to pristine MoS_2 (Figure 3C,D). The original black color of the solution was not significantly lost supporting the partial degradation and revealing higher stability to oxidation of functionalized MoS_2 sheets (Figure S7, Supporting Information). Additional TEM images confirming the clear changes in the morphology of the two MoS_2 nanomaterials from 0 to 30 d are shown in Figure S8 (Supporting Information).

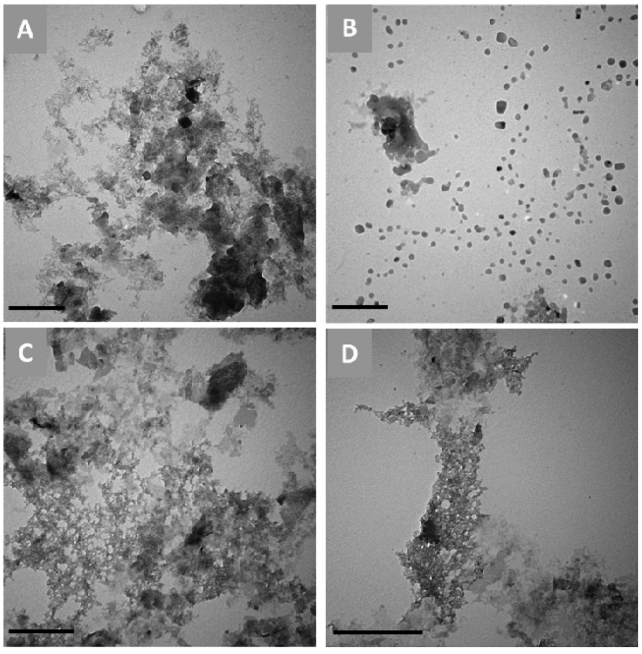

Figure 3. A,B) MoS_2 sheets after treating with 50×10^{-6} M of H_2O_2 for 14 d; C,D) *f*-MoS_2 sheets after treating with 50×10^{-6} M of H_2O_2 for 14 and 30 d, respectively. Scale bars correspond to 500 nm.

To extend the TEM analysis, we carried out high-resolution TEM (HRTEM) and selected area electron diffraction (SAED) studies to get more information about the morphological changes and crystallinity of both types of MoS_2 after treating with H_2O_2 for 30 and 60 d, respectively. HRTEM analyses revealed that 30 d treatment resulted into the transformation of pristine MoS_2 sheets into spherical nanoparticles of size between 5 and 30 nm (Figure S9A,B, Supporting Information). In addition, those nanoparticles are in polycrystalline state as measured by SAED analysis (Figure S9C,D, Supporting Information). Contrarily, degradation of *f*-MoS_2 sheets did not generate nanoparticles after 30 d (Figure S10A, Supporting Information), while a few fragments in the nanoscale range were observed after 60 d treatment (Figure S10B, Supporting Information), along with partially degraded and unmodified sheets (Figure S10C, Supporting Information). In addition, SAED pattern revealed that the remaining nanosheets (Figure S10C, Supporting Information) were single crystalline (Figure S10D, Supporting Information) and the resulted fragments were in amorphous state (Figure S10F, Supporting Information). Overall, TEM and HRTEM studies indicate that pristine MoS_2 sheets are highly sensitive to H_2O_2, while functionalized MoS_2 are more resistant. We have then checked the cytotoxic effects of the degraded products of MoS_2 and partially degraded *f*-MoS_2 after treating with 50×10^{-6} M of H_2O_2 for 14 and 30 d, respectively (vide infra).

2.4. Raman Analysis

To complement the electron microscopy results, we used Raman spectroscopy to understand the changes in the structure of MoS_2 and *f*-MoS_2 before and after the treatments with HRP, MPO, and hydrogen peroxide. TMDCs have two main Raman modes, corresponding to in-plane (E^1_{2g} at 386 cm^{-1}) and out-of-plane (A_{1g} at ≈406 cm^{-1}) vibrations.[11] In addition, J_1, J_2, and J_3 relative to the vibrations from S atoms are also present. J_1, J_2, and J_3 are identified at ≈147, 223, and 328 cm^{-1}, respectively, as displayed in **Figure 4**A (HRP 0 d).[7,39] The covalent functionalization clearly affected the Raman modes of MoS_2, since J_1 was split into two signals with a new peak at 167 cm^{-1}, and J_2 and J_3 strongly raised in relative intensity (Figure 4B, HRP 0 d). These changes are due to the covalent functionalization, where acetamide functional groups are bound to S atoms.[7] Significant changes were observed for pristine sample treated with HRP/H_2O_2 for 30 d, where J_2 peak became negligible and the intensity of J_1 and J_3 was reduced. Importantly, the intensities of both fundamental vibrations of MoS_2 (E^1_{2g} and A_{1g}) also diminished. These peaks were both missing after treatment with only H_2O_2 for 30 d (Figure 4A). In addition, J_2 and J_3 were completely absent, and a very broad signal was observed at 250–300 cm^{-1}, attributed to Mo—O—Mo deformation in MoO_3.[40–43] The absence of the fundamental peaks revealed that the lattice of MoS_2 crystals was strongly affected. Only a reduction of the intensities of these peaks was instead observed for *f*-MoS_2 treated with only H_2O_2 after 30 d (Figure 4B). *f*-MoS_2 sheets showed a moderate reduction in the intensities of Raman signals in the presence of the enzyme compared to 0 d, confirming the higher stability of functionalized MoS_2 toward

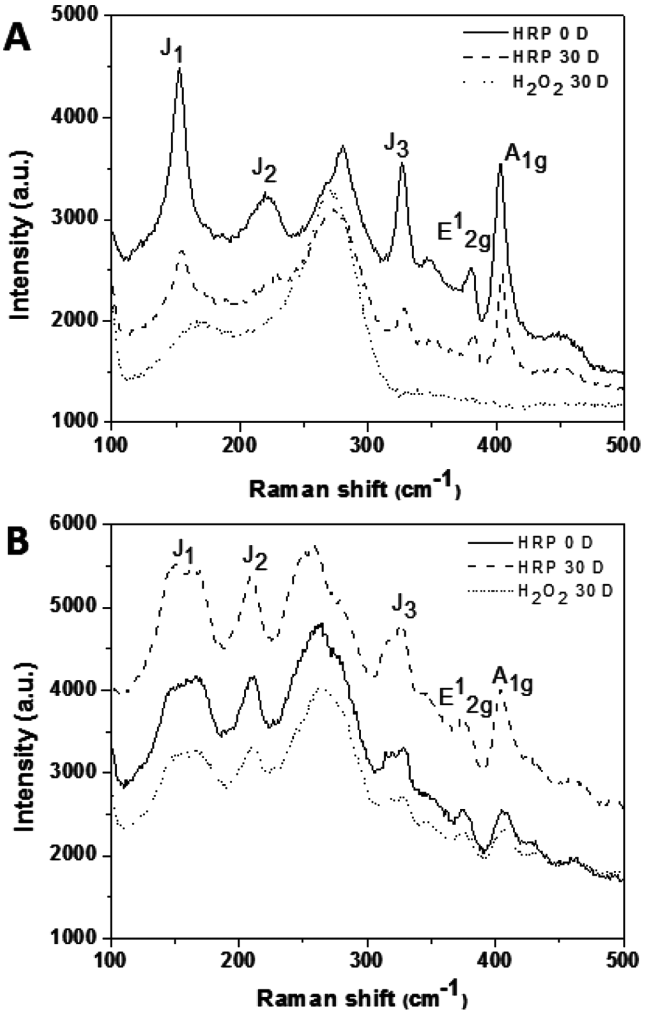

Figure 4. Raman analyses of HRP-treated MoS_2 and B) *f*-MoS_2 sheets, respectively.

HRP/H_2O_2 treatment. As J_1, J_2, and J_3 signals were related to the vibrations from S atoms,[39] the absence of these peaks after treating with H_2O_2, particularly for pristine material, can be attributed to the formation of MoO_3 as reported earlier for MoO_3 nanoparticles.[43]

In the case of the treatment of MoS_2 and *f*-MoS_2 with MPO/H_2O_2, the intensities of E^1_{2g} and A_{1g} gradually decreased (**Figure 5**). The Raman signatures for both MoS_2 samples are very weak after 24 h (see baseline corrected Raman spectra in Figures S11 and S12, Supporting Information), confirming that degradation by MPO was nearly completed. In the case of H_2O_2 alone treatment, the peroxide caused a higher damage to MoS_2 and *f*-MoS_2 compared to the control sample for HRP. Indeed, 200×10^{-6} M concentration of H_2O_2 was added every hour for 24 h in the control sample of MPO, while only 40×10^{-6} M of H_2O_2 was added every day for 30 d in the control sample of HRP. We would like to underline that the vibrations relative to S atoms are absent, likely confirming the formation of oxygenated species.[44]

In the third case corresponding to degradation using increasing concentrations of H_2O_2, we observed the changes in

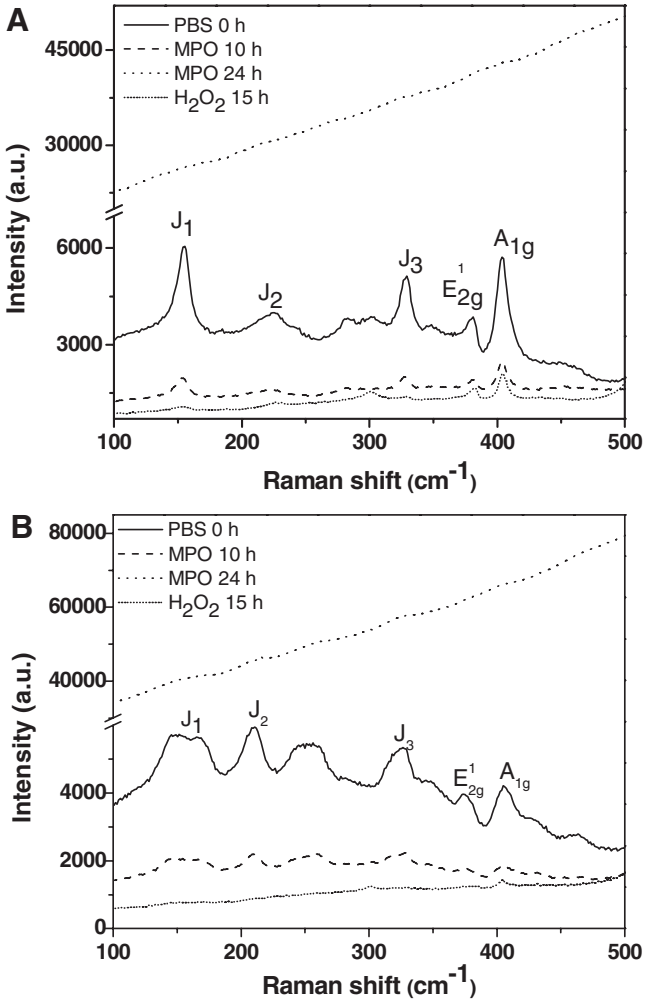

Figure 5. Raman analyses of A) MPO-treated MoS_2 and B) *f*-MoS_2 sheets, respectively.

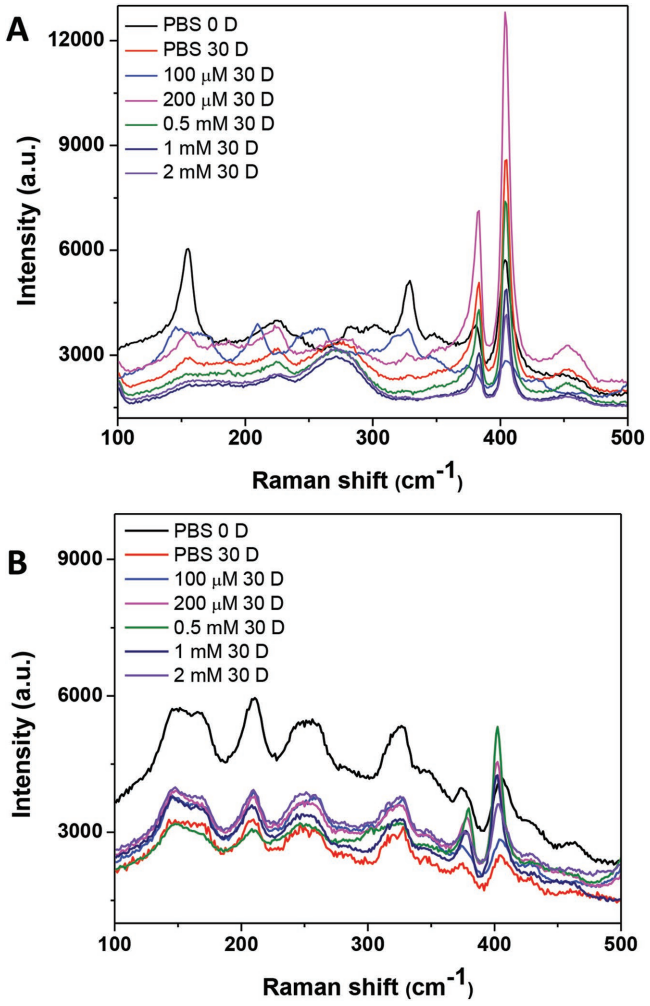

Figure 6. Raman analyses of A) MoS_2 and B) *f*-MoS_2 samples treated with different concentrations of hydrogen peroxide, respectively.

the Raman spectra after the treatment for 30 d (**Figure 6**A,B). For pristine MoS_2, the intensities of fundamental vibrations (E^1_{2g} and A_{1g}) are reduced gradually by increasing the concentrations of H_2O_2. Again, a broad peak around 250–300 cm^{-1} corresponding to Mo—O—Mo deformation appeared.[40–43] At the same time, also the vibrations relative to S atoms gradually diminished. At the highest concentrations, these peaks were completely absent, confirming the complete oxidation of MoS_2. The disappearance of J_1, J_2, and J_3 were not seen for *f*-MoS_2, while a general gradual reduction in the intensities of the bands was observed (Figure 6B). These results strongly confirmed the higher stability of functionalized MoS_2, as already observed by TEM (Figure 3).

2.5. X-Ray Photoelectron Spectroscopy Analysis

To get more details about the degree of oxidation of molybdenum during the degradation process, XPS analyses were conducted after treating the samples with HRP (30 d), MPO (24 h), and H_2O_2 alone (14 d for MoS_2 and 30 d for *f*-MoS_2, respectively) (**Figure 7** and Figure S13, Supporting Information). In all conditions, a complete oxidation of Mo(IV) in the pristine MoS_2 into Mo(VI) was confirmed by the presence of Mo^{VI} $3d_{3/2}$ (≈236.5 eV) and Mo^{VI} $3d_{5/2}$ (≈233 eV) in the Mo 3d high-resolution spectra (Figure 7A,C,E). In the case of *f*-MoS_2, the presence of mixture of Mo^{VI} 3d and Mo^{IV} 3d revealed instead an incomplete oxidation of *f*-MoS_2 sheets (Figure 7B,D,F). We would like to underline that in the starting MoS_2 and *f*-MoS_2, Mo^{VI} 3d peaks are absent (Figure S1, Supporting Information). The XPS results also support a higher resistance to oxidation of covalently functionalized MoS_2 compared to pristine sheets, in good agreement with Raman and TEM data. In addition, oxidation of S^{2-} into SO_4^{2-} was confirmed by XPS (Figure S13, Supporting Information). The peak at ≈168.5 eV corresponds to S 2p of SO_4^{2-} ions, and the two peaks at ≈161 and ≈162 eV are attributed to the binding energies of S 2p (S^{2-} $2p_{1/2}$ and S^{2-} $2p_{3/2}$, respectively) of MoS_2.[45] Sulfur atoms of pristine MoS_2 were oxidized to SO_4^{2-} ions, whereas in the cases of *f*-MoS_2, the mixture of S^{2-} and SO_4^{2-} were observed, as expected due to the incomplete oxidation of *f*-MoS_2 sheets.

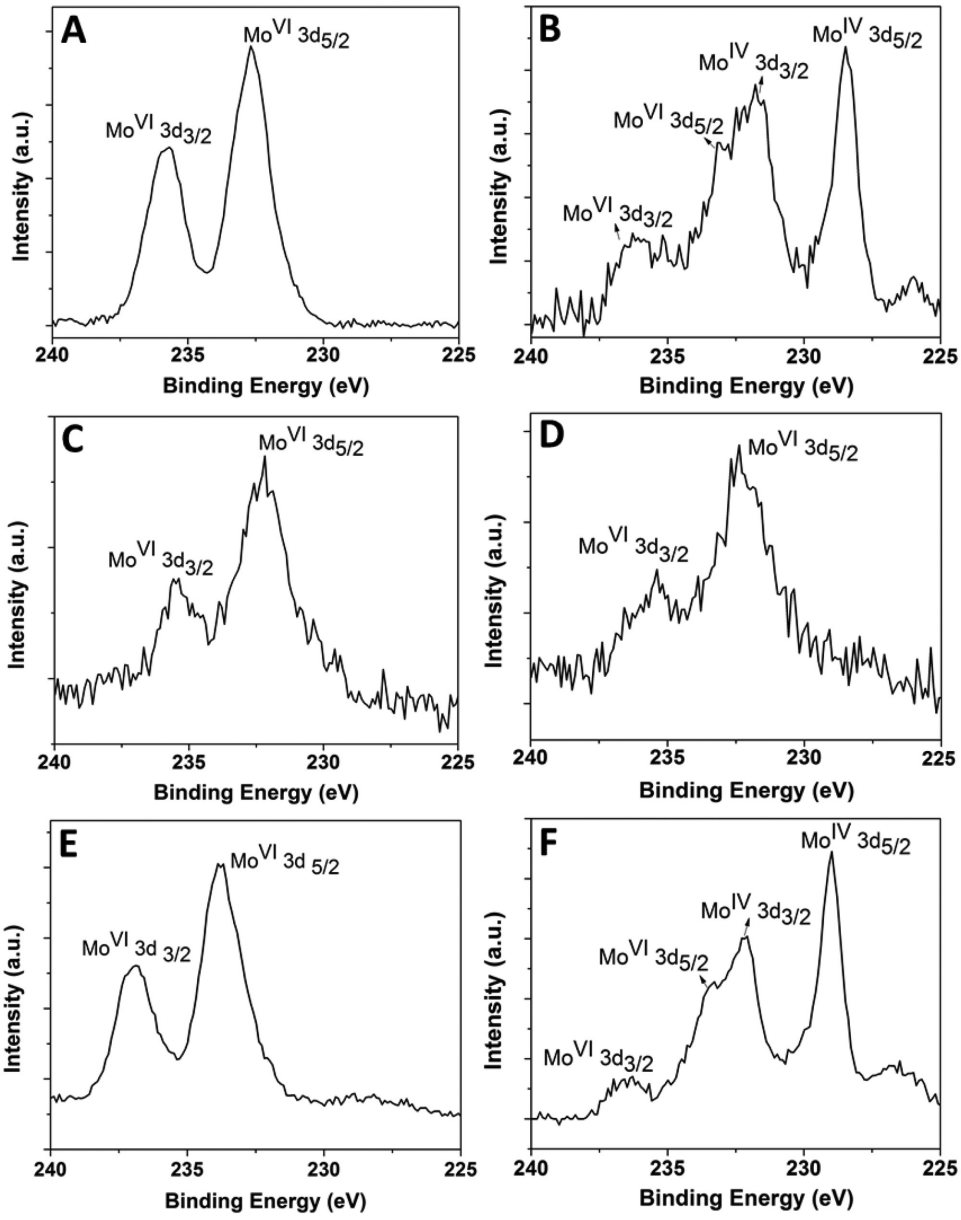

Figure 7. XPS analyses showing high-resolution spectra of Mo 3d binding energy of MoS_2 and *f*-MoS_2 treated with A,B) HRP+H_2O_2 (after 30 d), C,D) MPO+H_2O_2 (after 20 h), and E,F) H_2O_2 alone (after 14 d for MoS_2 and 30 d for *f*-MoS_2).

2.6. Mechanism of Degradation

The degradation trends of MoS_2 and *f*-MoS_2 by HRP, MPO, and H_2O_2 revealed that pristine MoS_2 is the most unstable in the aqueous solution. MoS_2 was even degraded in the PBS within three week incubation (see Figure S5, Supporting Information). The degradation of pristine MoS_2 was faster in the presence of H_2O_2 compared to the treatment with HRP or MPO, due to a quick oxidation of Mo(IV) into Mo(VI), most likely in the form of MoO_3 or MoO_4^{2-} ions.[19,46,47] The broad peak that we observed around 250–300 cm^{-1} (centered at ≈270 cm^{-1}) in the Raman spectra of pristine MoS_2 treated with HPR and H_2O_2 alone (Figures 4 and 6) corresponds to MoO_3 as described in the literature.[40–43] Indeed, it is well known that MoS_2 is oxidized to MoO_3 when treated with hydrogen peroxide.[46] However, in the case of MPO, which involve different oxidative intermediates (i.e., HOCl), the degradation process likely forms soluble MoO_4^{2-} ions.[38,47] Raman (Figures 4, 5, 6) and XPS analyses (Figure 7) confirmed that the degradation of MoS_2 lead the oxidation of molybdenum either into MoO_3 or soluble MoO_4^{2-} ions along with formation of SO_4^{2-} (see the corresponding equations in the Supporting Information).[46,48] Data in the literature further indicate that 1T phase of MoS_2 is metastable due to the richness in electrons, and it can be easily oxidized in the presence of salts, H_2O_2, oxygen, and moisture.[4,19,38,49] In addition, a more recent study also suggested that MoS_2 nanosheets can be transformed into soluble MoO_4^{2-} species once injected in mice. This study is of particular interest in the context of

biomedical applications of TDCMs. Indeed, the authors have demonstrated that the degradation of MoS_2 functionalized with polyethylene glycol (PEG) leads to an enhanced elimination rate in vivo. The degradation was confirmed by the generation of MoO_4^{2-} that was excreted within 30 d.[47] In view of the fast oxidation process found in our conditions, it will also be warranted to study in vivo degradation of our MoS_2 material. Raman analyses of MoS_2 nanosheets confirmed the presence of Mo—O bonds and the disappearance of the fundamental MoS_2 vibrations (E^1_{2g} and A_{1g}) after treating with H_2O_2 and MPO. In the case of MPO treatment, there is generation of HOCl along with MPO reactive intermediates, which are highly oxidants compared to reactive intermediates of HRP.[27,28] The chemical functionalization stabilized 1T phase of MoS_2 by converting the metallic character into the semiconductor state.[7] The degradation results of *f*-MoS_2 with HRP, MPO, and H_2O_2 revealed that the degradation was much slower when compared with pristine MoS_2, as confirmed by XPS analyses.

TMDCs are compounds different from carbon nanomaterials, and the degradation profile of MoS_2 nanosheets results different.[29,34,50] Carbon nanomaterials are completely oxidized by reactive intermediates of HRP or MPO whereas MoS_2 materials were more resistant. In contrast, MoS_2 samples are quickly degraded by H_2O_2. We expect that these materials could have different behavior during their interaction with body fluids or peroxidase enzymes and ROS under inflammation conditions. These materials may also have different fate compared to carbon materials, since they showed to be degraded even in the presence of moisture, salts, and ROS. In the next sections, we assessed the impact of both pristine and *f*-MoS_2 on various cell lines, primary immune cells, their interaction with cell membranes and uptake, and the cytotoxic effects of biodegradation products.

2.7. Cytotoxic Effects of MoS_2 and *f*-MoS_2

We have initially discussed the unprecedented advantages and superior performances of MoS_2 in the biomedical field.[3] Nevertheless, recent rapid advances in the use of new 2D nanomaterials for such purpose have raised important questions about their safety, similar to the earlier case of carbon nanotubes and graphene.[3,10] In order to identify new research directions, a critical evaluation of the possible toxicity of MoS_2 and its functionalized derivatives is needed. In vitro testing is the first crucial step in the road toward the approval of any new drugs or (bio)materials in the medical field.[18,37]

For these reasons we tried to unravel the possible cytotoxicity of MoS_2 and *f*-MoS_2 using two different cell lines and primary immune cells. We used HeLa cells as both nonphagocytic epithelial and cancer cell model and RAW 264.7 macrophages as immune and phagocytic model. Concerning primary immune cells, hMDMs were obtained by differentiating monocytes from healthy donors. These types of primary cells were used to evaluate the effects of MoS_2 and *f*-MoS_2 toward human immune cells. We carried out cell viability tests and measured primary cell activation and cytokine release as key cytotoxicity parameters.

The different cell types were exposed to increasing concentrations of MoS_2 or *f*-MoS_2 for 24 h. At the end of the incubation,

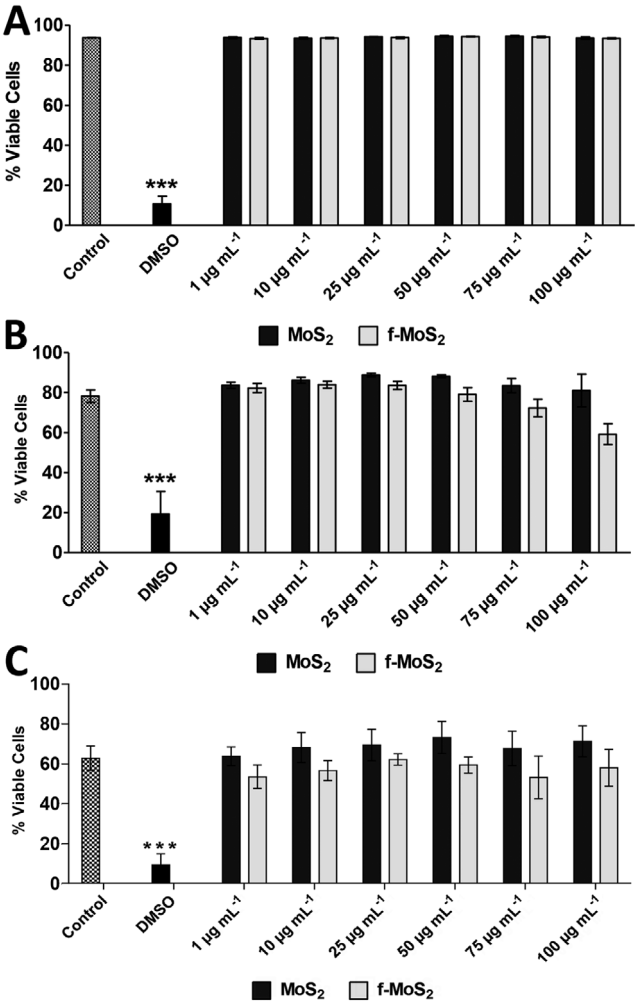

Figure 8. Flow cytometry analysis of A) HeLa, B) RAW 264.7, and C) hMDM cell viability exposed to different concentrations of MoS_2 or *f*-MoS_2 for 24 h. Two-way ANOVA followed by Bonferroni's post-test was performed to determine the statistical differences versus control cells and to compare MoS_2 and *f*-MoS_2 samples to each other (*$p < 0.05$; **$p < 0.01$; ***$p < 0.001$).

the cell viability was determined by flow cytometry. Our data revealed that the viability of HeLa cells was not affected by both MoS_2 samples, even at the highest concentration used, corresponding to 100 μg mL^{-1} (**Figure 8**A). Concerning RAW 264.7 macrophages, the viability was reduced to about 20% with respect to the control, but only at high concentrations and only in the case of *f*-MoS_2 (Figure 8B). Viability was not affected when the same cells were exposed to the pristine material. A similar behavior was observed for hMDMs as their healthy state was preserved within the entire concentration range of the two MoS_2 samples (Figure 8C) even when prolonging the exposure to MoS_2 and *f*-MoS_2 up to 7 d (Figure S14, Supporting Information).

Then we evaluated the impact of the two nanomaterials on the activation state of the immune cells. For this purpose, RAW 264.7 cells and hMDMs were exposed again to MoS_2 or *f*-MoS_2 for 24 h. After the incubation, the levels of expression of CD86, an important surface activation marker of antigen-presenting

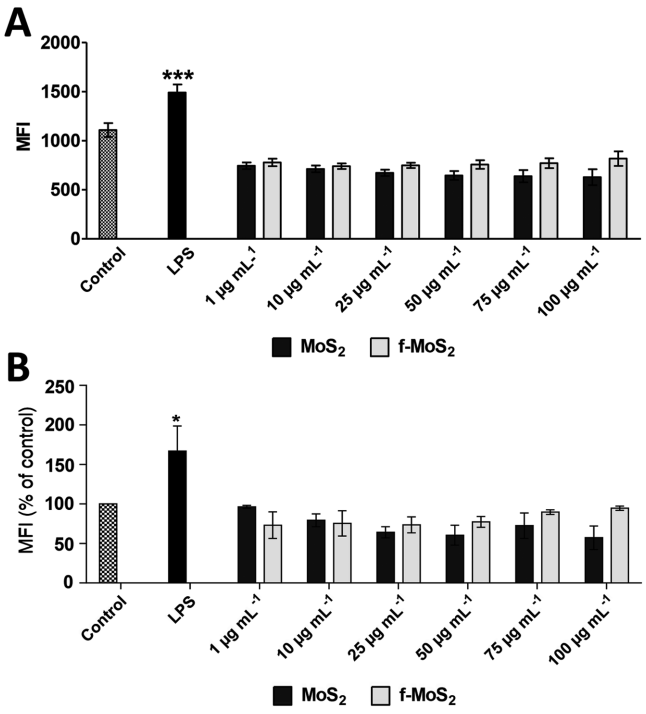

Figure 9. Flow cytometry analysis of CD86 surface expression in A) RAW 264.7 cells and B) hMDMs after exposure to different concentrations of MoS_2 or *f*-MoS_2 for 24 h. Two-way ANOVA followed by Bonferroni's post-test was performed to determine the statistical differences versus control cells and to compare MoS_2 and *f*-MoS_2 samples to each other (*$p < 0.05$; **$p < 0.01$; ***$p < 0.001$).

cells, were determined. Overall, the outcome of cell activation experiments on immune cells was consistent with cell viability results as no variation of CD86 levels in both RAW 264.7 cells and hMDMs was registered (**Figure 9**A,B). To further investigate a potential pro-inflammatory effect of our two MoS_2 samples, the secretion of two key pro-inflammatory cytokines (i.e., TNFα and IL6) by RAW 264.7 macrophages and hMDMs was analyzed. No significant amounts of cytokines were detected in RAW 264.7 cell supernatants (data not shown). Similarly, the quantity of TNFα secreted by hMDMs was comparable to basal levels (Figure S15, Supporting Information). Only at the highest concentration of pristine MoS_2 (100 μg mL^{-1}) we measured an increase of IL6 release although not significant.

The result of our first series of experiments on different types of cells suggests an encouraging overall absence of acute toxicity and pro-inflammatory activating effect of MoS_2 or *f*-MoS_2, up to a concentration of 50 μg mL^{-1}.

2.8. Cytotoxicity of MoS_2 and *f*-MoS_2 Degradation Products

We have shown how MoS_2 and *f*-MoS_2 can be degraded in test tube by naturally present enzymes and peroxides. In particular, a rather fast degradation with low concentration of H_2O_2 (i.e., 50×10^{-6} M) may occur, due to the natural overproduction of H_2O_2 by peroxidases.[21,22] Based on our degradation results in test tube (Figure 3, Figures S5 and S6, Supporting Information), we would expect that MoS_2 samples are also likely degraded in vivo by phagocytic and cancer cells. Reticuloendothelial system degradation by resident macrophages and tumor degradation might both contribute to the renal clearance and body elimination of MoS_2 thus reducing its accumulation in nontargeted organs and consequent cytotoxicity.[47] However, MoS_2 degradation products might exhibit cellular toxicity themselves, affecting, for example, clearance profile. As such possibility should not be ruled out, we decided to investigate the impact of the biodegradation products.

We started addressing this issue by performing cell viability and pro-inflammatory activation assays in cells exposed to MoS_2 and *f*-MoS_2 degradation products (named: MoS_2-DP and *f*-MoS_2-DP). Previous to cell exposure, the two material samples were treated (degraded) with 50×10^{-6} M H_2O_2 for 14 d (MoS_2-DP14 and *f*-MoS_2-DP14) or 30 d (*f*-MoS_2-DP30) (Figure S7, Supporting Information). As already mentioned in the previous paragraphs, H_2O_2 concentration was chosen in order to mimic the intracellular concentration of the

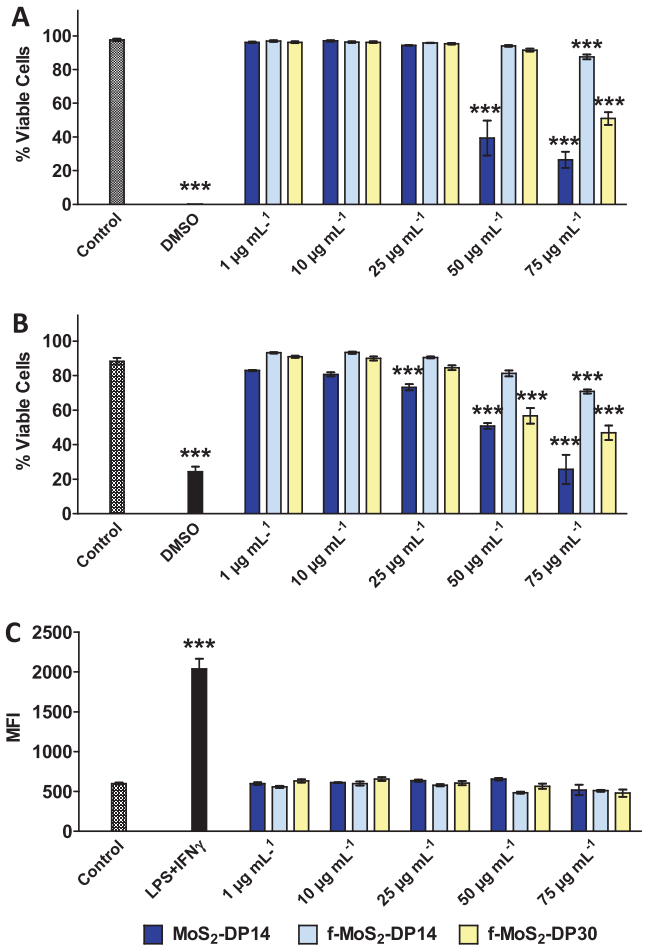

Figure 10. Flow cytometry analysis of cell viability in A) HeLa and B) RAW264.7 cells exposed to different concentrations of degraded MoS_2 or *f*-MoS_2 for 24 h. C) Flow cytometry analysis of the cell activation marker CD86 in RAW 264.7 cells after exposure to different concentrations of degraded MoS_2 or *f*-MoS_2 for 24 h. Two-way ANOVA followed by Bonferroni's post-test was performed to determine the statistical differences versus control cells (*$p < 0.05$; **$p < 0.01$; ***$p < 0.001$).

peroxide reported in the literature for leucocytes and cancer cells.[24,26] Cells were exposed for 24 h to MoS_2-DP14, *f*-MoS_2-DP14, or *f*-MoS_2-DP30 and subsequently analyzed by flow cytometry.

The outcome of cell viability experiments was similar for HeLa and RAW 264.7 cells. We observed a significant reduction of viable cells when they were exposed to concentrations equal to or greater than 50 μg mL^{-1} (HeLa) or 25 μg mL^{-1} (RAW 264.3) of pristine MoS_2-DP14 (**Figure 10**A,B). When the sample is functionalized (*f*-MoS_2-DP14), this effect is reduced in both cell lines (Figure 10A,B). However, when the functionalized compound is degraded for 30 d (*f*-MoS_2-DP30), toxicity starts to appear (Figure 10A,B), and it is more evident in the case of the macrophage cell line (a significant viability reduction is observed from 50 μg mL^{-1} of *f*-MoS_2-DP30).

These data suggest that the degradation products generated by pristine MoS_2 are cytotoxic at high concentrations. On the other hand, we have shown how, in cell-free degradation studies, *f*-MoS_2 was much more resistant to degradation by H_2O_2 compared to the pristine MoS_2 (Figure 3 and Figure S7, Supporting Information). We can conclude that functionalization stabilizes MoS_2, slowing down its degradation and attenuating the toxic effects of the degradation products.

Despite the adverse effect on cell viability, MoS_2-DPs and *f*-MoS_2-DPs did not trigger any pro-inflammatory response in macrophages. In fact, the expression of CD86 on the surface of RAW 264.7 cells did not increase after incubation with both degraded compounds (Figure 10C). Consistently, no pro-inflammatory cytokines were detected in the cell supernatants (data not shown). These data, apparently inconsistent with cell viability results, might be explained by the quick death of highly activated macrophages. As a consequence, CD86 could not be detected by flow cytometry and cytokines could not have been produced in time.

It is worth noting that the effects on viability are only due to the degradation products of MoS_2 and not to the presence of H_2O_2. In fact, by treating the cells with buffer solutions prepared in order to mimic the H_2O_2 concentration in the samples used for the experiments, cell viability was not impaired (Figure S16, Supporting Information).

2.9. Cellular Interaction and Internalization

Finally, to prove that the impact on cell viability and activation was due to the interaction and internalization of pristine and functionalized MoS_2 by the different cells, the uptake of these materials by HeLa cells and human monocyte-derived macrophages was investigated by TEM. For this purpose, the cells were exposed to 50 μg mL^{-1} of MoS_2 or *f*-MoS_2 for 24 h. The results showed a very efficient cell uptake of MoS_2 nanosheets, both pristine and functionalized, including the nonphagocytic HeLa cells. In **Figure 11**A–D (HeLa) and 11E,F (hMDMs), representative images of cells exposed to the MoS_2 samples for 24 h are shown. The materials were found both inside vesicles or free into the cytoplasm, behavior similar to graphene oxide.[51] This can be explained by the fact that MoS_2 and *f*-MoS_2 show a very high dispersibility in the aqueous media. In some cases, MoS_2 sheets penetrate the cell membrane as rolled needles (evidenced by a yellow arrow in Figure S17, Supporting Information), similar to carbon nanotubes and graphene oxide.[51,52]

Moreover, the formation of large invaginations of the cell membrane in correspondence to the materials indicates a probable internalization by ATP-dependent endocytic pathways

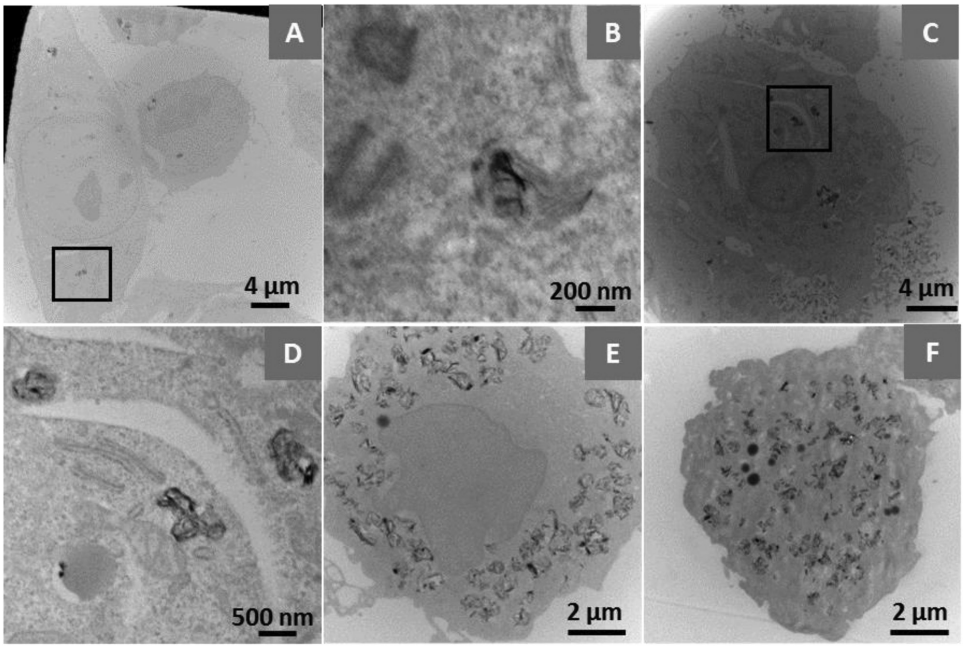

Figure 11. TEM images of A–D) HeLa cells and E,F) hMDMs incubated with MoS_2 or *f*-MoS_2 (50 μg mL^{-1}). HeLa cells incubated with A,B) MoS_2 and C,D) *f*-MoS_2 for 24 h, respectively. hMDMs incubated with E) MoS_2 and F) *f*-MoS_2 for 24 h, respectively. The red squares in the images are enlarged in the respective closed right panels.

(e.g., macropinocytosis or phagocytosis in the case of hMDM).[51] The hypothesis is also reinforced by the intracellular MoS_2-containing vesicles. On the other hand, the free nanosheets in the cytoplasm can be the results of passive diffusion through the plasma membrane or even endosome rupture.[51] There was not an evident difference in the mechanisms of the cell uptake between the pristine and the functionalized material for both HeLa and hMDM cells. Additional studies on the elucidation of the precise cell uptake mechanisms are warrant, but beyond the scope of this work.

3. Conclusion

In summary, this is the first report on biodegradation of different types of highly water dispersible MoS_2 (pristine and functionalized) nanosheets by enzymatic catalysis of peroxidases (i.e., plant HRP and human MPO) in the presence of low concentration of H_2O_2. Interestingly, much quicker degradation compared to peroxidase treatment was observed in biologically relevant concentrations of H_2O_2 without any enzymes. Slow degradation was also evidenced in simple buffer solution. Our results confirm very recent reports showing in vitro and in vivo degradability and elimination of MoS_2 nanosheets. In addition, covalent functionalization of MoS_2 tunes the degradation profile, which becomes particularly interesting in the design of advanced biomedical tools (i.e., drug delivery carriers or implants). Overall, these in vitro degradation and cellular toxicity studies suggest an enhanced biocompatibility and a better biodegradability of MoS_2 nanosheets, promoting this material as a better candidate for biomedical applications compared to other carbon or 2D nanomaterials. Finally, assessing in vivo toxicity and biodegradation of pristine and functionalized MoS_2 nanosheets is the objective of our future research.

Supporting Information

Supporting Information is available from the Wiley Online Library or from the author.

Acknowledgements

This work was supported by the Centre National de la Recherche Scientifique (CNRS), the Agence Nationale de la Recherche (ANR) through the LabEx project Chemistry of Complex Systems (ANR-10-LABX-0026_CSC), and the International Center for Frontier Research in Chemistry (icFRC). The authors gratefully acknowledge financial support from EU FP7-ICT-2013-FET-F GRAPHENE Flagship project (No. 604391). The authors wish to acknowledge Petra Hellwig and Frédéric Melin for giving access to Raman instrument, and Cathy Royer and Valérie Demais for TEM analyses at the Plateforme Imagerie in Vitro at the Center of Neurochemistry (Strasbourg, France). The authors would like to thank Dris Ihiawakrim for HRTEM and SAED measurements. We are also indebted to Fanny Bonacera for helping in preparing the graphics.

Received: October 5, 2016
Revised: November 13, 2016
Published online:

[1] M. Chhowalla, H. S. Shin, G. Eda, L.-J. Li, K. P. Loh, H. Zhang, *Nat. Chem.* **2013**, *5*, 263.
[2] P. Miró, M. Ghorbani-Asl, T. Heine, *Angew. Chem., Int. Ed.* **2014**, *53*, 3015.
[3] R. Kurapati, K. Kostarelos, M. Prato, A. Bianco, *Adv. Mater.* **2016**, *28*, 6052.
[4] J. Gao, B. Li, J. Tan, P. Chow, T.-M. Lu, N. Koratkar, *ACS Nano* **2016**, *10*, 2628.
[5] Y. Rong, K. He, M. Pacios, A. W. Robertson, H. Bhaskaran, J. H. Warner, *ACS Nano* **2015**, *9*, 3695.
[6] Q. Tang, D.-E. Jiang, *Chem. Mater.* **2015**, *27*, 3743.
[7] D. Voiry, A. Goswami, R. Kappera, C. de Carvalho Castro e Silva, D. Kaplan, T. Fujita, M. Chen, T. Asefa, M. Chhowalla, *Nat. Chem.* **2015**, *7*, 45.
[8] E. P. Nguyen, B. J. Carey, J. Z. Ou, J. van Embden, E. D. Gaspera, A. F. Chrimes, M. J. S. Spencer, S. Zhuiykov, K. Kalantar-zadeh, T. Daeneke, *Adv. Mater.* **2015**, *27*, 6225.
[9] E. P. Nguyen, B. J. Carey, C. J. Harrison, P. Atkin, K. J. Berean, E. Della Gaspera, J. Z. Ou, R. B. Kaner, K. Kalantar-zadeh, T. Daeneke, *Nanoscale* **2016**, *8*, 16276.
[10] D. Chimene, D. L. Alge, A. K. Gaharwar, *Adv. Mater.* **2015**, *27*, 7261.
[11] Y. Chen, C. Tan, H. Zhang, L. Wang, *Chem. Soc. Rev.* **2015**, *44*, 2681.
[12] C. Zhu, D. Du, Y. Lin, *2D Mater.* **2015**, *2*, 032004.
[13] E. L. K. Chng, Z. Sofer, M. Pumera, *Nanoscale* **2014**, *6*, 14412.
[14] K. Kalantar-zadeh, J. Z. Ou, T. Daeneke, M. S. Strano, M. Pumera, S. L. Gras, *Adv. Funct. Mater.* **2015**, *25*, 5086.
[15] X. Wang, N. D. Mansukhani, L. M. Guiney, Z. Ji, C. H. Chang, M. Wang, Y.-P. Liao, T.-B. Song, B. Sun, R. Li, T. Xia, M. C. Hersam, A. E. Nel, *Small* **2015**, *11*, 5079.
[16] W. Z. Teo, E. L. K. Chng, Z. Sofer, M. Pumera, *Chem. Eur. J.* **2014**, *20*, 9627.
[17] E. L. K. Chng, M. Pumera, *RSC Adv.* **2015**, *5*, 3074.
[18] K. Kostarelos, K. S. Novoselov, *Science* **2014**, *344*, 261.
[19] L. Dong, S. Lin, L. Yang, J. Zhang, C. Yang, D. Yang, H. Lu, *Chem. Commun.* **2014**, *50*, 15936.
[20] D. Trachootham, J. Alexandre, P. Huang, *Nat. Rev. Drug Discovery* **2009**, *8*, 579.
[21] H. Pelicano, D. Carney, P. Huang, *Drug Resist. Updates* **2004**, *7*, 97.
[22] Y.-T. Chiang, Y.-W. Yen, C.-L. Lo, *Biomaterials* **2015**, *61*, 150.
[23] M. Giorgio, M. Trinei, E. Migliaccio, P. G. Pelicci, *Nat. Rev. Mol. Cell Biol.* **2007**, *8*, 722.
[24] C. de Gracia Lux, S. Joshi-Barr, T. Nguyen, E. Mahmoud, E. Schopf, N. Fomina, A. Almutairi, *J. Am. Chem. Soc.* **2012**, *134*, 15758.
[25] H.-L. Pu, W.-L. Chiang, B. Maiti, Z.-X. Liao, Y.-C. Ho, M. S. Shim, E.-Y. Chuang, Y. Xia, H.-W. Sung, *ACS Nano* **2014**, *8*, 1213.
[26] K. E. Broaders, S. Grandhe, J. M. J. Fréchet, *J. Am. Chem. Soc.* **2011**, *133*, 756.
[27] V. Kagan, N. Konduru, W. Feng, B. Allen, J. Conroy, Y. Volkov, I. Vlasova, N. Belikova, N. Yanamala, A. Kapralov, Y. Tyurina, J. Shi, E. Kisin, A. Murray, J. Franks, D. Stolz, P. Gou, J. Klein-Seetharaman, B. Fadeel, A. Star, A. Shvedova, *Nat. Nanotechnol.* **2010**, *5*, 354.
[28] R. Kurapati, J. Russier, M. A. Squillaci, E. Treossi, C. Ménard-Moyon, A. E. Del Rio-Castillo, E. Vazquez, P. Samorì, V. Palermo, A. Bianco, *Small* **2015**, *11*, 3985.
[29] G. P. Kotchey, B. L. Allen, H. Vedala, N. Yanamala, A. A. Kapralov, Y. Y. Tyurina, J. Klein-Seetharaman, V. E. Kagan, A. Star, *ACS Nano* **2011**, *5*, 2098.
[30] A. R. Sureshbabu, R. Kurapati, J. Russier, C. Ménard-Moyon, I. Bartolini, M. Meneghetti, K. Kostarelos, A. Bianco, *Biomaterials* **2015**, *72*, 20.
[31] C. Bussy, C. Hadad, M. Prato, A. Bianco, K. Kostarelos, *Nanoscale* **2016**, *8*, 590.
[32] K. Bhattacharya, S. P. Mukherjee, A. Gallud, S. C. Burkert, S. Bistarelli, S. Bellucci, M. Bottini, A. Star, B. Fadeel, *Nanomed. Nanotechnol. Biol. Med.* **2016**, *12*, 333.
[33] R. Kurapati, C. Backes, C. Ménard-Moyon, J. N. Coleman, A. Bianco, *Angew. Chem., Int. Ed.* **2016**, *55*, 5506.

[34] B. L. Allen, P. D. Kichambare, P. Gou, I. I. Vlasova, A. A. Kapralov, N. Konduru, V. E. Kagan, A. Star, *Nano Lett.* **2008**, *8*, 3899.
[35] B. L. Allen, G. P. Kotchey, Y. Chen, N. V. K. Yanamala, J. Klein-Seetharaman, V. E. Kagan, A. Star, *J. Am. Chem. Soc.* **2009**, *131*, 17194.
[36] Y.-H. Fu, C.-Y. Chen, C.-T. Chen, *Polym. Chem.* **2015**, *6*, 8132.
[37] Z. Wang, W. Zhu, Y. Qiu, X. Yi, A. von dem Bussche, A. Kane, H. Gao, K. Koski, R. Hurt, *Chem. Soc. Rev.* **2016**, *45*, 1750.
[38] Z. Wang, A. von dem Bussche, Y. Qiu, T. M. Valentin, K. Gion, A. B. Kane, R. H. Hurt, *Environ. Sci. Technol.* **2016**, *50*, 7208.
[39] M. Calandra, *Phys. Rev. B* **2013**, *88*, 245428.
[40] K. S. Rabindar, G. B. Reddy, *J. Phys. D: Appl. Phys.* **2014**, *47*, 065305.
[41] K. Routray, W. Zhou, C. J. Kiely, W. Grünert, I. E. Wachs, *J. Catal.* **2010**, *275*, 84.
[42] M. M. Y. A. Alsaif, K. Latham, M. R. Field, D. D. Yao, N. V. Medehkar, G. A. Beane, R. B. Kaner, S. P. Russo, J. Z. Ou, K. Kalantar-zadeh, *Adv. Mater.* **2014**, *26*, 3931.
[43] P. Chandra, D. S. Doke, S. B. Umbarkar, A. V. Biradar, *J. Mater. Chem. A* **2014**, *2*, 19060.
[44] N. Kang, H. P. Paudel, M. N. Leuenberger, L. Tetard, S. I. Khondaker, *J. Phys. Chem. C* **2014**, *118*, 21258.
[45] X. Shao, J. Tian, Q. Xue, C. Ma, *J. Mater. Chem.* **2003**, *13*, 631.
[46] J.-M. Yun, Y.-J. Noh, C.-H. Lee, S.-I. Na, S. Lee, S. M. Jo, H.-I. Joh, D.-Y. Kim, *Small* **2014**, *10*, 2319.
[47] J. Hao, G. Song, T. Liu, X. Yi, K. Yang, L. Cheng, Z. Liu, *Adv. Sci.* **2017**, DOI:10.1002/advs.201600160.
[48] T. K. M. C. K. Gupta, *Hydrometallurgy in Extraction Processes*, Vol. *2*, CRC Press, Boca Raton, FL **1990**.
[49] M. Kan, J. Y. Wang, X. W. Li, S. H. Zhang, Y. W. Li, Y. Kawazoe, Q. Sun, P. Jena, *J. Phys. Chem. C* **2014**, *118*, 1515.
[50] I. I. Vlasova, A. A. Kapralov, Z. P. Michael, S. C. Burkert, M. R. Shurin, A. Star, A. A. Shvedova, V. E. Kagan, *Toxicol. Appl. Pharmacol.* **2016**, *299*, 58.
[51] J. Russier, E. Treossi, A. Scarsi, F. Perrozzi, H. Dumortier, L. Ottaviano, M. Meneghetti, V. Palermo, A. Bianco, *Nanoscale* **2013**, *5*, 11234.
[52] L. Lacerda, J. Russier, G. Pastorin, M. A. Herrero, E. Venturelli, H. Dumortier, K. T. Al-Jamal, M. Prato, K. Kostarelos, A. Bianco, *Biomaterials* **2012**, *33*, 3334.